Statistical and fractal analysis of nitrogen ion implanted tantalum thin films

A. H. Ramezani[1], S. Hoseinzadeh[2] and Zh. Ebrahiminejad[1]

[1]Department of Physics, West Tehran Branch, Islamic Azad University, Tehran, Iran
[2]Department of Mechanical and Aeronautical Engineering, Center for Asset Integrity Management, University of Pretoria, Pretoria, South Africa

*Correspondence to:

A. H. Ramezani (email: ramezani.1972@gmail.com) or

S. Hoseinzadeh (email: Hoseinzadeh.siamak@gmail.com)

Abstract

Tantalum bulk has been implanted by nitrogen ions at an energy30 keV and at various doses of 1×10^{17}, 3×10^{17}, and 10×10^{17} ions/cm^2. As a result, thin films are rough; their morphology and stochastic properties have been investigated. The monofractal analysis is done for unimplanted and implanted samples based on the statistical analysis conception. The correlation function and also the correlation length of the samples have been studied. Also, the power spectral density, the dimension of the fractal, the distribution of height, and the skewness and kurtosis (the higher-order moments) of the surface height have been investigated. The results show the deviation of height distribution from the gaussian one. The measurement of jagged and irregularity of samples have been investigated by calculating the roughness exponent and fractal dimensions. The rough samples which have been produced by ion bombardment have the self-affine fractal properties.

Keywords: Tantalum bulk · Nitrogen ion implantation · Monofractal analysis · Fractal dimension

Introduction

Titanium has suitable mechanical properties, low density, and excellent biocompatibility, high corrosion resistance. Therefore, for many years, titanium was used extensively in experimental works because of its technological applications [1,2,3,4]. Various researches have been motivated to improve the titanium characteristics, such as sputtering model, ion coating, and ion implantation. The ion implantation method has been frequently used because it introduces other chemical types and generates imperfections in target materials [5,6,7,8]. Carbon, nitrogen, and oxygen have been used to improve the surface of the titanium. The hardness wears resistance, and corrosion resistance of Tantalum surfaces usually improves by nitrogen ion implantation and allows the film growth process to keep the substrate at low or adequate temperatures [9,10,11]. By nitrogen implantation techniques, the titanium nitride can be formed on titanium surfaces. The characteristics of the samples provided by the atomic force microscopy (AFM), the x-ray diffraction (XRD), and the scanning electron microscopy (SEM) images. There are several methods such as 'blanket' fractal analysis [12], 'skyscraper' fractal analysis [13], and the box-counting method

[14] for investigation on the fractality behavior of the experimentally generated thin films [15,16,17,18].

Recently, the effect of nitrogen ion implantation on structural and mechanical characteristics of tantalum investigated [19]. Here, it is interesting to study the morphology of implanted and unimplanted tantalum samples. Based on the monofractal analysis, the height fluctuations, the higher-order moments (skewness, and kurtosis), power spectral density, correlation function, and correlation length of samples have been calculated. Also, the roughness exponent and the fractal dimension's samples have been valued.

The present paper is ordered as follows. In Sect. 2, thin film preparation and AFM analysis are presented. In Sect. 3, the statistical analysis is presented, and the measurements and discussions are described. The summarized remarks are expressed in Sect. 4.

Thin film preparation and AFM analysis

In the present section, the process of ion implantation on tantalum samples, which do in Plasma Physics Research Center (PPRC), Science and Research Branch, is explained. The minutiae of the procedure are as following; the tantalum samples which cut into 1 cm × 1 cm and 0.58 mm thickness exposed to nitrogen ion implantation. The nitrogen ions land on the sample vertically, and their energy was 30 keV. The doses of (99.999%) were considered 1×10^{17}, 3×10^{17}, and 10×10^{17} ions/cm^2 at ambient temperature. Through the nitrogen ion bombardment, which leads to heat transfer, the maximum steady value of room temperature reached 100 ºC. The ion beams cover the entire sample surface uniformly, because of the range of ions doses.

The samples were polished and then ultrasonically cleaned in alcohol and acetone to have the glossy samples. The extracted ions were accelerated to the maximum energy of 30 keV. Among the implanted ions and surface of tantalum samples, the angle is considered 90°. Through the implantation procedure, the sample temperature measures by a thermocouple.

In all cases, the ion beam energy and current densities have been considered fixed. The parameters which are used during the ion implantation have been presented in Table 1. The I_{corr} (corrosion's current), the temperature and E_{corr} (corrosion's Potential) take the fixed values 100 μA/cm^2, 100 K and 30 KeV for all samples, correspondingly.

Table 1 The parameters of ion implantation process

Sample	Fluxes (ions/cm^2)	Time (s)
1	Unimplanted	0
2	1×10^{17}	375
3	3×10^{17}	480
4	10×10^{17}	1500

The AFM results of samples as a roughness variation are presented in Fig. 1.

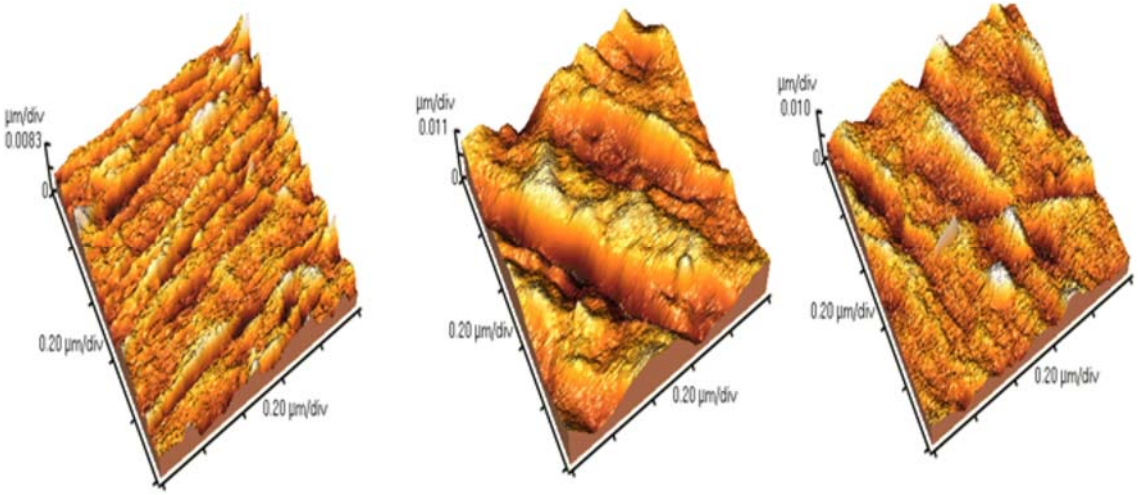

Fig. 1. The AFM images of unimplanted, 1×10^{17}, and 3×10^{17} samples from left to right

Statistical and fractal analysis

In this paper, the change of surface morphology and roughness has been evaluated by using the (AFM) analysis. Also, the stochastic properties and fractal behavior of implanted and unimplanted tantalum samples have been investigated to characterize the morphology of the sample. The implanted samples were exposed to nitrogen ion implantation.

The fractal concepts have been used to explore the morphology of rough samples. These surfaces are called stochastic because respect to the smooth plane, their height fluctuations are random. The RMS height is well-defined as Eq. 1:

$$\sigma = \sqrt{h(r)^2}, \tag{1}$$

where h(r)h(r) is the height at position *r* [20].

The RMS roughness (RqRq) of samples are displayed in Table 2.

Table 2 The RMS roughness height of unimplanted and implanted samples

Sample	**1**	**2**	**3**	**4**
σ	1.667	4.119	2.142	3.786

The RMS height cannot describe the rough surface because the surfaces with the same σ have different morphology. Therefore, to analyse the samples morphology, the correlation function, $C(\ell)$, is studied. This function describes the manner of heights variations laterally to the samples surfaces. It applied to describe the correlation property of surface heights at two different positions that are ℓ point away. The normalized $C(\ell)$ is defined as Eq. 2.

$$C(\ell) = \langle h(r_1)\, h(r_2) \rangle / \sigma^2, \quad (2)$$

Which $\ell = |r_1 - r_2|$. Based on this definition, for points with large distance, $C(\ell)$ becomes zero. The correlation length, ξ, is defined as the distance which $C(\ell)$ drops 1/*e* of its original value [21, 22]. The correlation function, $C(\ell)$ of unimplanted and implanted samples respect to the separation distance ℓ showed in Figs. 2, and 3. The correlation function has the same behavior in all cases. By the results, the, $C(\ell)$, reduces by increasing of ℓ value and also it has the same behavior in two cases.

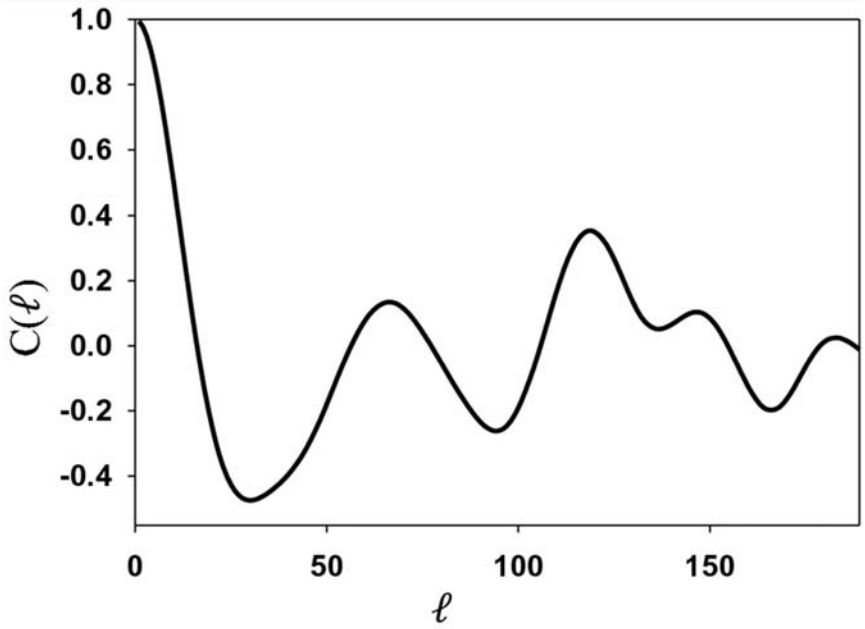

Fig. 2. Correlation function as separation distance for unimplanted sample

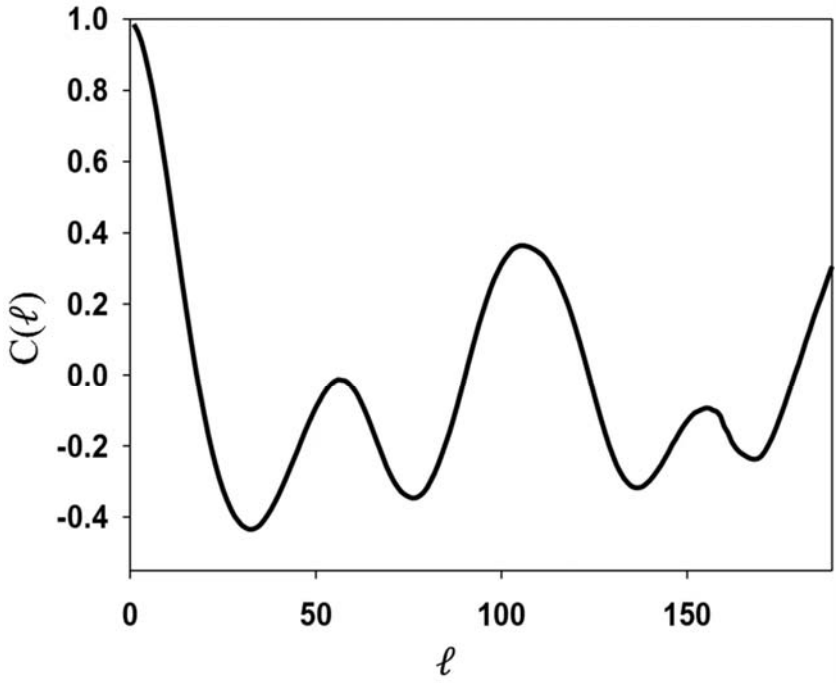

Fig. 3. Correlation function as separation distance for sample 3

Figure 4 shows the variation of correlation length as a function of nitrogen dose. As it is seen in the figure, the correlation length increases with increasing the ion dose.

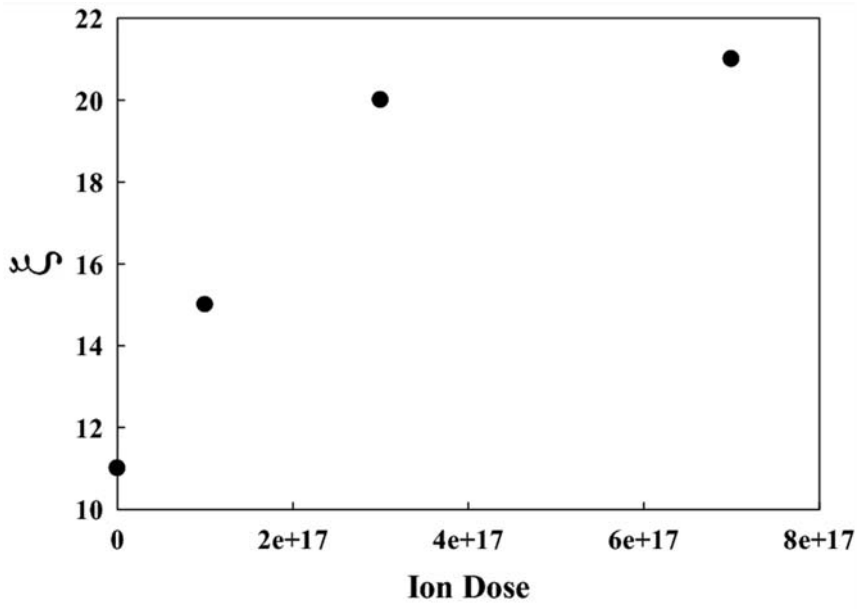

Fig. 4. Correlation length versus ion dose

In other words, as the ion doses increases, the rough surface produced are more correlated.

Surface height distribution

For the monofractal analysis, the symmetry of the height or deviation from the Gaussian distribution has been studied. Therefore, the height distribution of samples surfaces and the 3rd- and 4th-order moments (two higher-order moments) have been investigated to access to the information about the surface morphology.

The 3rd moment of height distribution is named skewness. The skewness is a reason of the symmetry distribution (Eq. 3):

$$R_{sk} = \frac{\left\langle \left(h - \bar{h}\right)^3 \right\rangle}{\left\langle (h - \bar{h})^2 \right\rangle^{3/2}}. \tag{3}$$

Skewness sign indicates that the data points are skewed to the right (positive sign) or to the left (negative sign) of the data average [23].

The 4th-order moment of surface height is the kurtosis. In the case of Gaussian distribution, $R_{ku} = 3$. The kurtosis is a measure of the sharpness of the height distribution function (Eq. 4). In other words it determines the fatness ($R_{ku} < 3$) or the sharpness ($R_{ku} > 3$) peak of the probability, and it defined as [23]:

$$R_{\mathrm{ku}} = \frac{\left\langle \left(h - \bar{h}\right)^4 \right\rangle}{\left\langle (h - \bar{h})^2 \right\rangle^2}. \tag{4}$$

The results show that both skewness and kurtosis of unimplanted and implanted samples show the deviation of Gaussian distribution. The skewness is negative for implanted samples ($R_{sk} = -1.01$), and it is positive for the unimplanted sample ($R_{sk} = 1.001$). Also, the measure of kurtosis shows the nonconformity from the Gaussian distribution (where $R_{ku} = 3$). The results show that $R_{ku} = 2.98$ for implanted and unimplanted samples. The ($R_{ku} < 3$) indicates the few valleys and further high peaks over the samples. Also, the deviation from the Gaussian distribution have been proofed by the asymmetric tail and nonzero skewness measures [24, 25].

Besides the higher-order moments of height distribution, a suitable measure that describes the extent of the heights overhead the mean surface and the height variation alongside the surface is the power spectrum (Fig. 5). The power spectrum is the transform of the correlation function and mathematically defined as Eq. 5:

$$P(k) = \frac{1}{2\pi} \int C(\ell)\, \mathrm{e}^{ik.\ell} \mathrm{d}\ell. \tag{5}$$

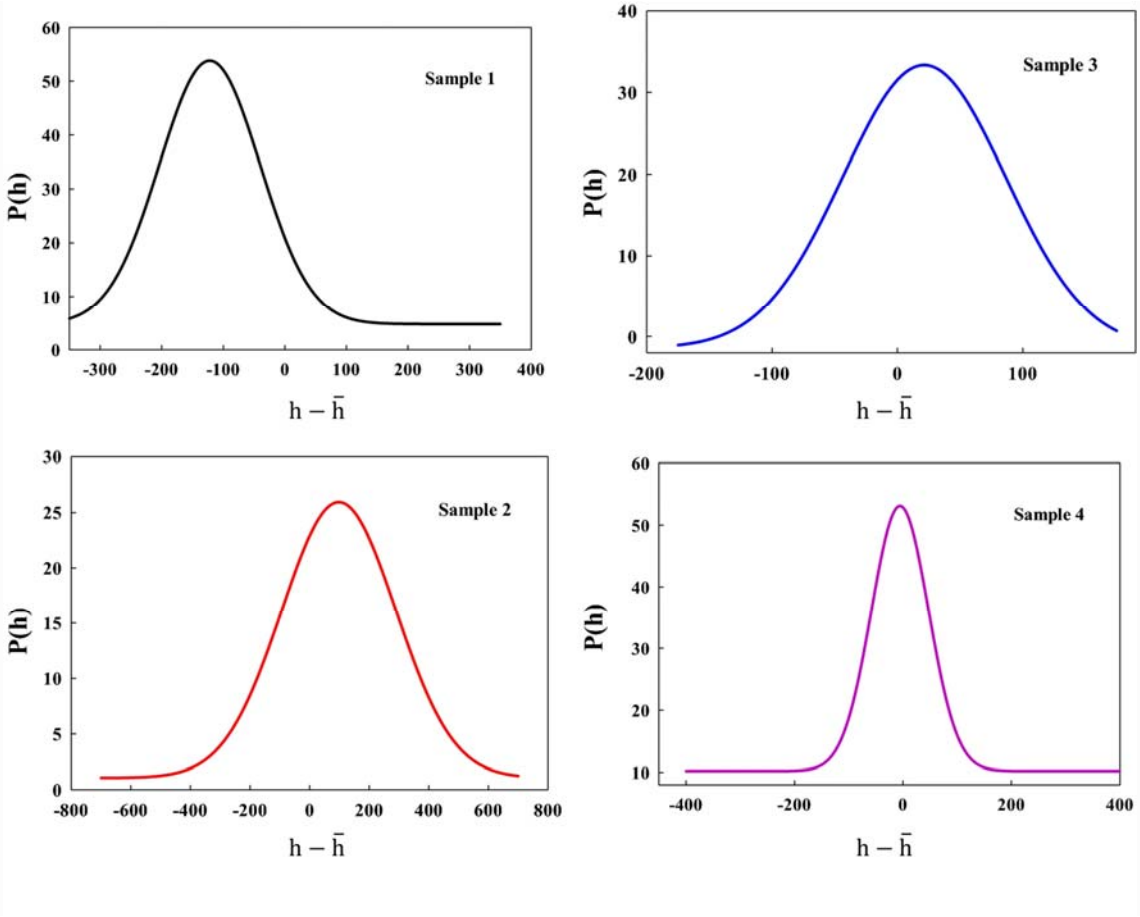

Fig. 5. The normalized height distribution for unimplanted and implanted samples

The normalized height distribution *P*(*h*) has been evaluated when the height of the sites is measured regarding the mean height [25].

It shows the deviation of the distribution from the Gaussian one, which confirms the results of skewness and kurtosis.

Roughness exponent and fractal dimension

The width of rough surfaces is defined as Eq. 6:

$$w(L,t) = \sqrt{\left\langle \left(h(i,t) - \bar{h}(t)\right)^2 \right\rangle}, \tag{6}$$

where *h*(*i*,*t*) is the height of the surface at site *i* and the time *t*. *h* (*t*) is the average amount of height at time *t*. When a surface becomes saturated inadequate long times, the width of roughness (*w*) shows a power low dependency on substrate size (*L*) as $w_L = L^{\alpha}$ [20]. The Roughness exponent αα, also called Hurst exponent is used to analyze the smoothness

and roughness of the surfaces. In other words, it designates the irregularity of saturated rough surface [26, 27].

For a self-affine surface, this scaling exponent is in the range $0 \leq \alpha \leq 1$. The self-affine characteristic indicates that a surface appears less rough as the scale increases. In other words, if a profile is self-affine, a magnified portion of it will appear statistically identical to the entire profile if different magnifications are used. The roughness exponent of samples has been measured and displayed in Table 3. The small values of roughness exponent characterize jagged or irregular surfaces at short length scales [26, 27]. Our results show that the irregularity of unimplanted samples is less than the others. Also, as the dose of ion implantation increases, the jagged of the sample's surface varied.

Table 3 The roughness exponent of unimplanted and implanted samples

Sample	1	2	3	4
Roughness exponent	0.803	0.545	0.613	0.875

The other measurement which is straightly related to roughness exponent is the fractal dimension, DfDf, which is a measure of the surface complexity. Among the several approaches of calculating the fractal dimension [28], one can obtain$Df=E+1-\alpha Df=E+1-\alpha$. The

the fractal dimension of samples has been calculated and presented in Table 4.

Table 4 The fractal dimension of unimplanted and implanted samples

Sample	1	2	3	4
*D*f	1.197	1.455	1.387	1.125

Erosion by ion bombardment of surfaces is a way of producing rough surfaces with self-affine fractal properties. Ion bombardment (sputtering) of an iron surface produced a surface which was self-affine fractal [33]. Based on the obtained results, it can be concluded that these unimplanted and implanted rough samples have the fractal behavior.

Summary

In conclusion, a monofractal analysis has been applied to study the morphology of rough surfaces. These tantalum bulks were unimplanted or implanted by nitrogen ion-implanted. Based on our results, the correlation length increases with increasing the ion dose. This result shows that implanted samples are more correlated than uncorrelated ones. Also, the measurements of skewness and kurtosis showed the deviation from Gaussian distribution. This deviation has been confirmed by plotting the normalized height distribution. Also, the roughness exponent and fractal dimension of samples have been calculated. The monofractal analysis has revealed that the samples which have been studied in present work are the self-affine fractal surfaces. Our results were in high-grade agreement with experimental results.

References

1. A.H. Ramezani, S. Hoseinzadeh, A. Bahari, J. Inorg. Organomet. Polym. Mater. **28**, 847 (2018)

2. S. Hoseinzadeh, A.H. Ramezani, J. Nanoelectron. Optoelectron. **14**, 1413 (2019)

3. A.H. Ramezani, S. Hoseinzadeh, Zh Ebrahiminejad, Mod. Phys. Lett. B (2020). https://doi.org/10.1142/S0217984920501638

4. S. Hoseinzadeh, A.H. Ramezani, J. Nanostruct. **9**, 276 (2019)

5. K. Alves de Souza, A. Robin, Mater. Chem. Phys. **103**, 351 (2007)

6. A.N. Protsenko, Nucl. Instrum. Methods Phys. Res. Sect. B **82**, 417 (1991)

7. M. Esmaeelpour, G. Kavei, Appl. Surf. Sci. **252**, 6353 (2006)

8. S. Picard, J.B. Memet, R. Sabot, J.L. Grosseau, J.P. Riviere, R. Meilland, Mater. Sci. Eng. A **303**, 163 (2001)

9. G.S. Chen, S.T. Chen, J. Appl. Phys. **87**, 8473 (2000)

10. J. Chuang, M. Chen, Thin Solid Films **322**, 213 (1998)

11. M. Stavrev, D. Fischer, C. Wenzel, K. Drescher, N. Mattern, Thin Solid Films **79**, 307 (1997)

12. T. Gredig, E.A. Silverstein, M.P. Byrne, J. Phys. Conf. Ser. **417**, 012069 (2013)

13. V.N. Bliznyuk, V.M. Burlakov, H.E. Assender, G.A.D. Briggs, Y. Tsukahara, Macromol. Symp. **167**, 89 (2001)

14. A. Le Gal, L. Guy, G. Orange, Y. Bomal, M. Kluppel, Wear **264**, 606 (2008)

15. D. Raoufi, F. Hosseinpanahi, Appl. Phys. **7**, 21 (2013)

16. K. Ghosh, R.K. Pandey, Appl. Phys. A **125**, 98 (2019)

17. K. Ghosh, R.K. Pandey, AIP Conf. Proc. **2115**, 030280 (2019)

18. K. Ghosh, R.K. Pandey, Mater. Res. Express **6**, 086454 (2019)

19. A.H. Ramezani, M.R. Hantehezadeh, M. Ghoranneviss, E. Darabi, Appl. Phys. A **122**, 178 (2016)

20. A.L. Barabasi, H.E. Stanley, *Fractal Concepts in Surface Growth* (Cambridge University Press, New York, 1995)

21. J.A. Ogilvy, J.R. Foster, J. Phys. D: Appl. Phys **22**, 1243 (1989)

22. I. Simonovski, L. Cizelj, International Conference. Nuclear Energy for New Europe, 110.1 (2005)

23. Y. Zhao, G.-C. Wang, T.-M. Lu, *Characterization of Amorphous and Crystalline Rough Surface: Principles and Applications* (Department of Physics, Applied Physics, and Astronomy Rensselaer Polytechnic Institute Troy, New York, 2001)

24. D. Raoufi, F. Hosseinpanahi, J. Theor. Appl. Phys. **7**, 21 (2013)

25. W.-Z. Wang, H. Chen, Y.-Z. Hu, H. Wang, Tribol. Int **39**, 522 (2006)

26. G. Palasanzas, J. Barnas, Phys. Rev. B **56**, 7726 (1997)

27. G. Palasantzas, J. Barnasa, ThM De Hosson, J. Appl. Phys. **88**, 927 (2000)

28. B.N.J. Persson, Tribol Lett **54**, 99 (2014)

29. R.P. Yadav, T. Kumar, A.K. Mittal et al., Appl. Surf. Sci. **347**, 706 (2015)

30. D. Dastan, Appl. Phys. A **123**, 699 (2017)

31. S. Hoseinzadeh, R. Ghasemiasl, A. Bahari et al., J. Electron. Mater. **47**, 3552 (2018)

32. S. Hoseinzadeh, R. Ghasemiasl, A. Bahari et al., J. Mater. Sci. Mater. Electron. **28**, 14446 (2017)

33. J. Krim, I. Heyvaert, C. Van Haesendonck, Y. Bruynseraede, Phys. Rev. Lett. **70**, 57 (1993)